



Shahid Chamran  
University of Ahvaz

# Journal of Applied and Computational Mechanics



## Research Paper

# An Impact of Induced Magnetic and Cattaneo-Christov Heat Flux Model on Nanofluid Flow across a Stretching Sheet

K.M. Nihaal<sup>1</sup>, U.S. Mahabaleshwar<sup>1</sup>, L.M. Pérez<sup>2</sup>, P. Cattani<sup>3</sup>

<sup>1</sup> Department of Studies in Mathematics, Shivagangotri, Davangere University, Davangere, India,  
E-mail: nihaal.kmdvg@gmail.com (K.M.N.); u.s.m@davangereuniversity.ac.in (U.S.M.)

<sup>2</sup> Departamento de Física, FACY, Universidad de Tarapacá, Casilla 7D, Arica, 1000000, Chile, E-mail: lperez@academicos.uta.cl

<sup>3</sup> Department of Computer, Control and Management Engineering, University of Rome "La Sapienza", Via Ariosto 25, 00185 Roma, Italy,  
E-mail: cattani.1642354@studenti.uniroma1.it

Received November 30 2023; Revised January 14 2024; Accepted for publication February 11 2024.

Corresponding authors: K.M. Nihaal (nihaal.kmdvg@gmail.com), U.S. Mahabaleshwar (u.s.m@davangereuniversity.ac.in)

© 2024 Published by Shahid Chamran University of Ahvaz

**Abstract.** The induced magnetic field is used to control the fluid motion and heat transfer in a variety of applications, such as in MHD devices, microfluidics, electrically conducting fluids in channels and in circular pipes, and clinical applications such as drug delivery and cooling of nuclear reactors. Henceforth this investigation aims to elucidate the behavior of viscoelastic (second-grade fluid) ternary nanofluid flow through a permeable stretching sheet with an induced magnetic field. The stretching surface is subjected to the Cattaneo-Christov heat and mass flux model to investigate heat and mass transfer properties. Solutions of reduced governing equations are obtained numerically via the shooting method and computed using the bvp-4c algorithm. The impacts of diverse active parameters such as porous medium, magnetic parameter, reciprocal magnetic Prandtl parameter, stretching parameter, HSS parameter, and relaxation time parameter for heat and mass flux are studied graphically. In addition, the values of significant engineering factors are calculated and comparative analysis is presented through bar graphs. It is seen that regular heat sink/source promotes thermal distribution and relaxation time for mass flux enhances the mass transfer rate between fluid flow and solid surface.

**Keywords:** Ternary nanofluid; Porous medium; Heat source/sink; Induced magnetic field; Modified Cattaneo-Christov model.

## 1. Introduction

The word nanofluid refers to a developed colloidal blend of a base fluid and a mono sort of nanoparticle. Choi and Eastman [1] were the first researchers to do a study regarding the thermal properties of this theory. Highly developed electronics, radiators, photovoltaic cells, and technical micro apparatuses are constantly constrained by inefficient thermal control approaches, which are mostly caused by sporadic thermal production in the system. Hence a better understanding of ternary nanofluid has gained the attention of many eminent scholars that attributed to its remarkable upgrades of thermal performance and efficiency in the transmission of heat and it seems that the results of numerous studies [2-4] appeared captivating and informative. Recently, Maranna et al. [5] explored the impacts of radiation and HSS on ternary viscoelastic fluid.

Porous media pique the interest of academics and researchers not only because of their composition but also because several approaches have been proposed to improve their efficacy and speed up heat transmission. A lot of scholars are interested in the applications of fluid motion and heat transfer through a porous medium in a broad range of industrial and physiological areas such as filtration, oil extraction, and purification [6-7]. Mahabaleshwar et al. [8] considered permeable stretching/shrinking sheet for the investigation of the effect of MHD and radiation over an axisymmetric non-Newtonian flow. The heat source/sink plays a key part in forecasting the heat transfer characteristics of fluid flows. As a result, it has become a prominent concept in heat transport analysis [9-12]. Awaludin et al. [13] examined a heat and mass transfer analysis over a porous stretching /shrinking surface in proximity to the stagnation point with HSS effects. Acharya and Mabood [14] carried out a comparative analysis of the hydrothermal properties of HNF and NF past a smooth bent surface with the influence of HSS. Sneha et al. [15] investigated a study of entropy generation in the presence of HSS, and radiation over a MHD stretching sheet with CNT.

A magnetic field has industrial applications in proton chemical shifts in aromatic compounds, the magnetism of macroscopic devices, and biomedical operations such as MRI and MRT [16-17]. Using the Darcy Brinkman model, Kopp et al. [18] explored thermal convection in a porous media under an external magnetic field. In their research for better thermal performance, they considered the combination of nanofluids and microorganisms. Utilizing a magnetic field, Khan et al. [19] conducted a study on blood flow



incorporating gold nanoparticles over a curved permeable surface in the vicinity of partial slip and radiation. Sheremet et al. [20] investigated the natural convection of an unstable fluid flow in a wavy-walled chamber under the influence of a magnetic field using the mathematical nanofluid model given by Buongiorno.

Many researchers are showing fantastic energy in exploring heat propagation applications in engineering and industrial operations, such as the cooling of nuclear reactors and of spacecraft, energy production, use of magnetic drugs for drug delivery, food technology, and many others. Over 200 years ago, Fourier [21] was a pioneering researcher who investigated heat transport behaviour in many different situations. Cattaneo [22] proposed an extension of Fourier's law to heat conduction in an inflexible body. To propose the Maxwell-Cattaneo law, he modifies Fourier's law by incorporating the thermal relaxation time term. Christov [23] developed a material invariant version of Cattaneo's model with the aid of Oldroyd's upper-convected derivative. Jamshed et al. [24] investigated the effects of radiative flux, shape effects, and entropy analysis upon a heated slippery unstable surface containing HNF. In his research, he used Cattaneo-Christov heat flux model. In the presence of chemical reaction and radiation, Rehman et al. [25] inspected the effects of Cattaneo-Christov heat flux over Darcy-Frochheimer of Sutterby nanofluid flow over a stretching sheet.

According to the above-mentioned review, the TNF has significant applications in various domains (engineering and industrial) because of its greater heat transfer rate compared to the conventional fluids. This work is the extension of the study conducted by Hayat et al. [26] where they have explored the influence of induced magnetic field over second grade fluid over a stretching surface with a convective boundary. However, the previous researchers did not consider the CC heat flux model. The novelty of the present research is to explore the combined impacts of induced magnetic field and CC heat fluxing over Second-grade TNF fluid flow. The authors have investigated the model with  $Ni-ZnFe_2O_4$ ,  $Mn-ZnFe_2O_4$ , and  $Fe_2O_4$  suspended with ethylene glycol and water. This study is a worthy combination due to the following advantages:

- The above-mentioned ferromagnetic nanofluids have the potential to enhance heat transfer such as in heated pipes and fin-tube heat exchangers.
- The ferromagnetic nanofluids have advantages over conventional fluids in heat transfer analysis due to their additional advantage property i.e., external magnetic field.

## 2. Mathematical Model and Solution

Here a steady, laminar, C-C heat flux, conducting second-grade fluid with three nanoparticles  $Ni-ZnFe_2O_4$ ,  $Mn-ZnFe_2O_4$ , and  $Fe_2O_4$  over a stretching surface is taken into account. The temperatures at the surface and at ambient fluid are  $T = T_w$  and  $T = T_\infty$ .  $C = C_w$  and  $C = C_\infty$  denote the wall concentration and concentration at the far field, respectively. The geometry of the present study is presented in Fig. 1. In the physical problem, the following considerations are given:

- Horizontal linear permeable stretching sheet with uniform velocity  $u_w(x)$ .
- Induced magnetic field aspects are considered.
- Heat source/sink is valid.

The main governing PDEs are [26-28]:

$$\frac{\partial u}{\partial x} + \frac{\partial v}{\partial y} = 0, \quad (1)$$

$$\frac{\partial H_1}{\partial x} + \frac{\partial H_2}{\partial y} = 0, \quad (2)$$

$$u \frac{\partial u}{\partial x} + v \frac{\partial u}{\partial y} = u_e \frac{\partial u_e}{\partial x} + \nu_{nf} \frac{\partial^2 u}{\partial y^2} + \frac{\alpha_1}{\rho_{nf}} \left( u \frac{\partial^3 u}{\partial x \partial y^2} + \frac{\partial u}{\partial x} \frac{\partial^2 u}{\partial y^2} + \frac{\partial u}{\partial y} \frac{\partial^2 v}{\partial y^2} + v \frac{\partial^3 u}{\partial y^3} \right) + \frac{\mu_f}{4\pi\rho_{nf}} \left[ (H_1) \frac{\partial H_1}{\partial x} + (H_2) \frac{\partial H_2}{\partial y} \right] - \frac{\mu_f}{4\pi\rho_{nf}} \left( (H_\infty) \frac{dH_\infty}{dx} \right) - \frac{\nu_{nf}}{K^*} u, \quad (3)$$

$$u \left( \frac{\partial H_1}{\partial x} \right) + v \left( \frac{\partial H_2}{\partial y} \right) - \left[ \left( \frac{\partial u}{\partial x} \right) H_1 + \left( \frac{\partial v}{\partial y} \right) H_2 \right] = \zeta_1 \frac{\partial^2 H_2}{\partial y^2}, \quad (4)$$

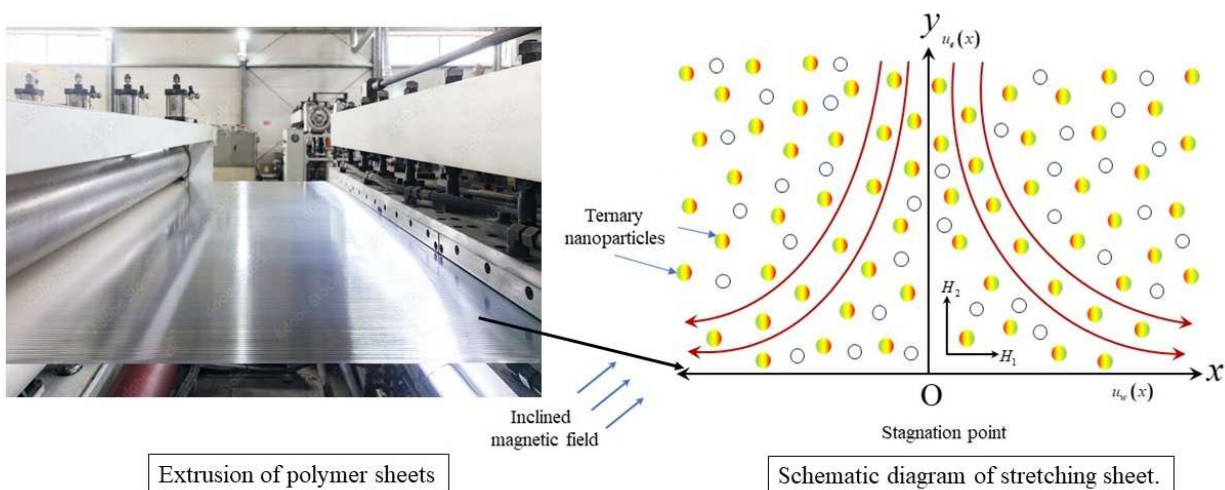


Fig. 1. The geometry of the present study.



$$u \frac{\partial T}{\partial x} + v \frac{\partial T}{\partial y} = \frac{K_{\text{tnf}}}{(\rho C_p)_{\text{tnf}}} \frac{\partial^2 T}{\partial y^2} - \varepsilon_T \left( u \frac{\partial u}{\partial x} \frac{\partial T}{\partial x} + v \frac{\partial v}{\partial y} \frac{\partial T}{\partial y} + u \frac{\partial v}{\partial x} \frac{\partial T}{\partial y} + v \frac{\partial u}{\partial y} \frac{\partial T}{\partial x} + 2uv \frac{\partial^2 T}{\partial x \partial y} + u^2 \frac{\partial^2 T}{\partial x^2} + v^2 \frac{\partial^2 T}{\partial y^2} \right) + \frac{Q_0(T - T_\infty)}{(\rho C_p)_{\text{tnf}}}, \quad (5)$$

$$u \frac{\partial C}{\partial x} + v \frac{\partial C}{\partial y} = D \frac{\partial^2 C}{\partial y^2} - \varepsilon_c \left( u \frac{\partial u}{\partial x} \frac{\partial C}{\partial x} + v \frac{\partial v}{\partial y} \frac{\partial C}{\partial y} + u \frac{\partial v}{\partial x} \frac{\partial C}{\partial y} + v \frac{\partial u}{\partial y} \frac{\partial C}{\partial x} + 2uv \frac{\partial^2 C}{\partial x \partial y} + u^2 \frac{\partial^2 C}{\partial x^2} + v^2 \frac{\partial^2 C}{\partial y^2} \right). \quad (6)$$

The relative BCs. are given by:

$$u = U_w, \quad v = 0, \quad \frac{\partial H_1}{\partial y} = H_2 = 0, \quad T = T_w, \quad C = C_w, \quad \text{at } \eta = 0, \quad (7)$$

$$u \rightarrow u_\infty(x), \quad \frac{\partial u}{\partial y} = 0, \quad H_1 \rightarrow H_\infty, \quad T \rightarrow T_\infty, \quad C \rightarrow C_\infty, \quad \text{as } \eta \rightarrow \infty. \quad (8)$$

From Eqs. (1-8), the terms  $u$  and  $v$  represent the velocity components along  $x$  and  $y$  directions, respectively.  $\nu$ ,  $\mu$ , and  $\rho$  are the kinematic viscosity, effective dynamic viscosity, and density, respectively.  $(H_1, H_2)$  are the components of induced magnetic field and  $H_0$  is the ambient estimation for magnetic field.  $K^*$  is the permeability factor and  $\zeta_1$  denotes the magnetic diffusivity.  $\varepsilon_T$  and  $\varepsilon_c$  represent the relaxation time for heat and mass flux, respectively.  $K$  and  $C_p$  are the thermal conductivity and specific heat component and  $Q_0$  is the HHS parameter.

The effective characteristics of ternary nanoparticles are as follows [29]:

$$(\rho C_p)_{\text{tnf}} = \left( \frac{(\rho C_p)_{s1} \phi_1}{(\rho C_p)_f} + (1 - \phi_1) \left[ (1 - \phi_2) \left( (1 - \phi_3) + \frac{(\rho C_p)_{s3} \phi_3}{(\rho C_p)_f} \right) + \frac{(\rho C_p)_{s2} \phi_2}{(\rho C_p)_f} \right] \right) (\rho C_p)_f,$$

$$\mu_{\text{tnf}} = \frac{\mu_f}{(1 - (\phi_1 + \phi_2 + \phi_3))^{2.5}}, \quad \rho_{\text{tnf}} = (1 - \phi_1) \left[ (1 - \phi_2) \left[ (1 - \phi_3) \rho_f + \rho_{s3} \phi_3 \right] + \rho_{s2} \phi_2 \right] + \rho_{s1} \phi_1,$$

$$k_{\text{tnf}} = \left( \frac{k_{s1} + 2k_{\text{hnf}} - 2\phi_1(k_{\text{hnf}} - k_{s1})}{k_{s1} + 2k_{\text{hnf}} + \phi_1(k_{\text{hnf}} - k_{s1})} \right) k_{\text{hnf}}, \quad k_{\text{hnf}} = \left( \frac{k_{s2} + 2k_{\text{nf}} - 2\phi_2(k_{\text{nf}} - k_{s2})}{k_{s2} + 2k_{\text{nf}} + \phi_2(k_{\text{nf}} - k_{s2})} \right) k_{\text{nf}},$$

$$k_{\text{nf}} = k_f \left( \frac{k_{s3} + 2k_f - (\phi_3 k_f - \phi_3 k_{s3})}{k_{s3} + 2k_f + (\phi_3 k_f - \phi_3 k_{s3})} \right).$$

The employed similarity transformations are:

$$\eta = \sqrt{\frac{a}{\nu}} y, \quad u = ax f'(\eta), \quad v = -\sqrt{\nu a} f(\eta), \quad \theta = \frac{T - T_\infty}{T_w - T_\infty}, \quad (9)$$

$$\chi = \frac{C - C_\infty}{C_w - C_\infty}, \quad H_1 = H_0 x g'(\eta), \quad H_2 = -H_0 \sqrt{\frac{\nu}{a}} g(\eta).$$

After using Eq. (9), we have:

$$\frac{1}{A_1 A_2} f'''' + A^2 - f'^2 + f f'' + \hat{k} (2f' f''' - f''^2 - f f''') + \frac{\beta^*}{A_2} [g g'' + 1 - g'^2] - \frac{\varepsilon}{A_1 A_2} f' = 0, \quad (10)$$

$$\zeta g''' + f g'' - g f'' = 0, \quad (11)$$

$$\frac{A_4}{A_3} \frac{1}{\text{Pr}} \theta'' + f \theta' - \gamma_1 (f f' \theta' + f^2 \theta'') + \frac{\text{Ni}}{A_3} \theta = 0, \quad (12)$$

$$\frac{1}{\text{Sc}} \chi'' + f \chi' - \gamma_2 (f f' \chi' + f^2 \chi'') = 0. \quad (13)$$

and corresponding obtained BCs. are:

$$\text{at } \eta = 0: \quad f'(0) = 1, \quad f(0) = 0, \quad g(0) = 0, \quad g''(0) = 0, \quad (14)$$

$$\text{as } \eta \rightarrow \infty: \quad f'(\infty) = A, \quad g'(\infty) \rightarrow 1, \quad f''(\infty) = 0, \quad \theta(\infty) = 0, \quad \chi(\infty) = 0. \quad (15)$$

where,



$$A_1 = (1 - \phi_1 - \phi_2 - \phi_3)^{2.5},$$

$$A_2 = (1 - \phi_1)^{2.5} \left[ (1 - \phi_2) \left[ (1 - \phi_3) + \frac{\rho_{s3}}{\rho_f} \phi_3 \right] + \frac{\rho_{s2}}{\rho_f} \phi_2 \right] + \frac{\rho_{s1}}{\rho_f} \phi_1,$$

$$A_3 = \left[ \frac{(\rho C_p)_{s1} \phi_1}{(\rho C_p)_f} + (1 - \phi_1) \left[ (1 - \phi_2) \left[ (1 - \phi_3) + \frac{(\rho C_p)_{s3} \phi_3}{(\rho C_p)_f} \right] + \frac{(\rho C_p)_{s2} \phi_2}{(\rho C_p)_f} \right] \right],$$

$$A_4 = k_{\text{trf}} / k_f,$$

where,

$A = \frac{c}{a}$  - stretching parameter,

$\hat{k} = \frac{\alpha_1 a}{\nu \rho}$  - second grade nanofluid parameter,

$\beta^* = \frac{\mu_e H_0^2}{4\pi c^2 \rho_f}$  - magnetic parameter,

$\zeta = \frac{\mu_e}{\nu_f}$  - reciprocal magnetic Prandtl number,

$\varepsilon = \frac{\nu a}{K}$  - porosity parameter,

$\text{Pr} = \frac{\nu}{k}$  - Prandtl number,

$\gamma_1 = \varepsilon_1 a$  and  $\gamma_2 = \varepsilon_c a$  are thermal and concentration relaxation parameters, respectively,

$\text{Ni} = \frac{Q_0}{a(\rho C p)_f}$  - HSS parameter,

$\text{Sc} = \frac{\nu}{D}$  - Schmidt number.

The engineering gradients of current problem are  $C_f$  (Skin-friction),  $Nu$  (Nusselt number), and  $Sh$  (Sherwood number) which are defined as [27]:

$$C_{fx} = \frac{\tau_w}{\rho u_w^2}, \quad \tau_w = \left[ \alpha_1 \left( u \frac{\partial^2 u}{\partial x \partial y} + 2 \frac{\partial u}{\partial y} \frac{\partial u}{\partial x} + v \frac{\partial^2 u}{\partial y^2} \right) + \mu_{\text{trf}} \frac{\partial u}{\partial y} \right]_{y=0}, \quad (16)$$

$$Nu_x = \frac{x q_w}{(T_w - T_\infty)}, \quad q_w = -k_{\text{trf}} \left( \frac{\partial T}{\partial y} \right)_{y=0}, \quad (17)$$

$$Sh_x = \frac{x q_c}{(C_w - C_\infty)}, \quad q_c = - \left( \frac{\partial C}{\partial y} \right)_{y=0}. \quad (18)$$

Utilizing Eq. (9) and Eqs. (14-16), yields:

$$C_{fx} (\text{Re})^{1/2} = \left[ \frac{f''(0)}{A_1} + \beta^* (3f'(0) + f''(0) - f(0)f'''(0)) \right], \quad (19)$$

$$Nu_x (\text{Re})^{-1/2} = - \frac{k_{\text{trf}}}{k_f} \theta'(0), \quad (20)$$

$$Sh_x (\text{Re})^{-1/2} = -\chi'(0). \quad (21)$$

### 3. Computational Procedure

The computational tool `bvp-4c` followed by shooting method was utilized to find the solution of reduced Eqs. (10-13) and boundary conditions (14-15). The simplified equations are reduced to first order system. For this, we have considered:

$$f = h(1), f' = h(2), f'' = h(3), f''' = h(4)$$

$$g = h(5), g' = h(6), g'' = h(7)$$



$$\theta = h(8), \theta' = h(9)$$

$$\chi = h(10), \chi' = h(11)$$

$$h'(4) = \frac{1}{Ky(1)} \left( \frac{h(4)}{A_1 A_2} + K(2h(2)h(4) - h(3)^2) + h(1)h(3) - h(2)^2 + \frac{\beta^*}{A_2} \left( h(5)h(7) + 1 - h(6)^2 - \frac{\varepsilon}{A_1 A_2} h(2) \right) \right) \quad (22)$$

$$h'(7) = -\frac{1}{\zeta} (h(1)h(7) - h(5)h(3)) \quad (23)$$

$$h'(9) = -\frac{1}{\left( \frac{A_4}{A_3} - \gamma_1 h(1)^2 \right)} \left( h(1)h(9) - \gamma_1 h(1)h(2)h(9) + \frac{Ni}{A_3} h(8) \right) \quad (24)$$

$$h'(11) = -\frac{1}{\left( \frac{1}{Sc} - \gamma_2 h(1)^2 \right)} (h(1)h(9) - \gamma_2 h(2)h(1)h(11)) \quad (25)$$

with

$$h(2)_0 - 1, h(1) = 0, h(5)_0 = 0, h(7)_0 = 0, \quad (26)$$

$$h(2)_\infty - A, h(6)_\infty - 1, h(3)_\infty = 0, h(8)_\infty = 0, h(10)_\infty = 0. \quad (27)$$

The transformed IVP equations (22)-(27) are solved numerically by using bvp-4c package using thermophysical properties of base fluid and nanoparticles given in Table 1. Additionally, identical results were obtained when the numerical solutions are compared to those from earlier studies in Tables 2 and 3. The computation is carried out by varying parameters  $A = 1$ ,  $\beta^* = 0.1$ ,  $\varepsilon = 0.3$ ,  $\zeta = 0.1$ ,  $Ni = 0.5$ ,  $\gamma_1 = \gamma_2 = 0.1$ , and  $Sc = 0.6$ .

#### 4. Results and Discussion

The variations in the fluid velocity profile ( $f'$ ) for the diverse magnitudes of porosity parameter ( $\varepsilon$ ) is indicated in Fig. 2. The values of  $f'$  decline gradually with an augmentation in the values of  $\varepsilon$ . Lower permeability is caused primarily by a rise in a value of the porosity variable, which results in an overall reduction in velocity. Physically, an increase in the porosity characteristic causes the porous material to hinder the flow of liquid, slowing its movement. As a result, the thickness of the boundary layer decreases, and the velocity profiles drop fast. It is seen that decrease in water is more when compared to ethylene glycol (Eg). The effect of variation in  $\beta^*$  over  $f'$  and  $g'$  are examined in Fig. 3 and Fig. 4. It depicts that  $f'$  and  $g'$  decelerates for upsurge values of  $\beta^*$  in both water and Eg. From a physical stand point, an increase in the magnetic parameter builds resistance in the flow due to the Lorentz force generation. Impact of  $\beta^*$  is more in water than in Eg.

**Table 1.** Thermophysical characteristics of nanoparticles and base fluid [30-31].

| Properties                  | Ni-ZnFe <sub>2</sub> O <sub>4</sub> | Mn-ZnFe <sub>2</sub> O <sub>4</sub> | Fe <sub>2</sub> O <sub>4</sub> | H <sub>2</sub> O | Eg     |
|-----------------------------|-------------------------------------|-------------------------------------|--------------------------------|------------------|--------|
| $\rho$ (kgm <sup>-3</sup> ) | 4800                                | 4700                                | 5180                           | 997.1            | 1116.6 |
| $C_p$ (J / kgK)             | 710                                 | 1050                                | 670                            | 4179             | 2382   |
| $k$ (W / mk)                | 6.3                                 | 3.9                                 | 9.7                            | 0.613            | 0.249  |
| Pr                          | -                                   | -                                   | -                              | 6.2              | 204    |

**Table 2.** Validation of the code for  $f''(0)$  and different values of A when  $A_1 = A_2 = 1$ ,  $\hat{k} = \beta^* = \varepsilon = 0$ .

|      | $f''(0)$ [32] | $f''(0)$ Present study |
|------|---------------|------------------------|
| A    |               |                        |
| 0.10 | -9694         | -9692                  |
| 0.20 | -9181         | -9180                  |
| 0.50 | -0.6673       | -0.6671                |
| 2.00 | 2.0175        | 2.0174                 |
| 3.00 | 4.7293        | 4.7292                 |

**Table 3.** Validation of the code for  $-\theta'(0)$  and different values of A when  $A_4 = A_3 = 1$ ,  $\gamma_1 = Ni = 0$ .

| $-\theta'(0)$ [32] |       |       |       |       | $-\theta'(0)$ Present study |       |       |       |
|--------------------|-------|-------|-------|-------|-----------------------------|-------|-------|-------|
| Pr                 |       |       |       |       | Pr                          |       |       |       |
| A                  | 0.05  | 0.5   | 1.0   | 1.5   | 0.05                        | 0.5   | 1.0   | 1.5   |
| 0.1                | 0.081 | 0.383 | 0.603 | 0.777 | 0.080                       | 0.382 | 0.604 | 0.775 |
| 0.2                | 0.099 | 0.408 | 0.625 | 0.797 | 0.010                       | 0.406 | 0.624 | 0.796 |
| 0.5                | 0.136 | 0.473 | 0.692 | 0.863 | 0.135                       | 0.471 | 0.691 | 0.862 |
| 1.0                | 0.178 | 0.563 | 0.796 | 0.974 | 0.177                       | 0.562 | 0.795 | 0.972 |
| 2.0                | 0.241 | 0.709 | 0.974 | 1.171 | 0.242                       | 0.707 | 0.973 | 1.170 |
| 3.0                | 0.289 | 0.829 | 1.124 | 1.341 | 0.288                       | 0.827 | 1.121 | 1.340 |



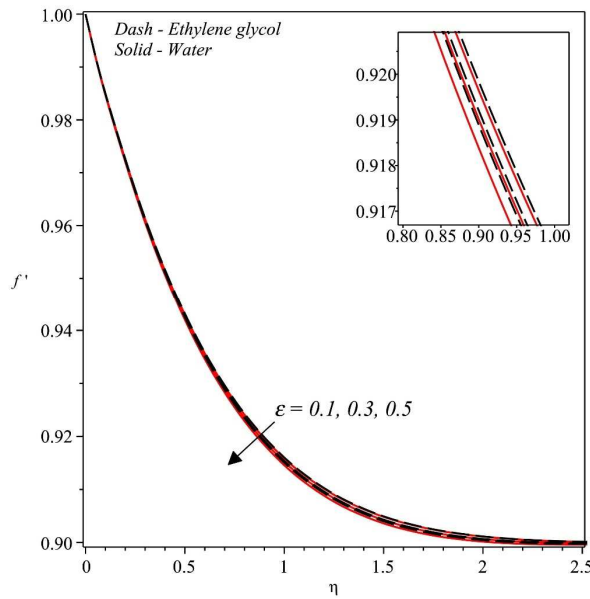
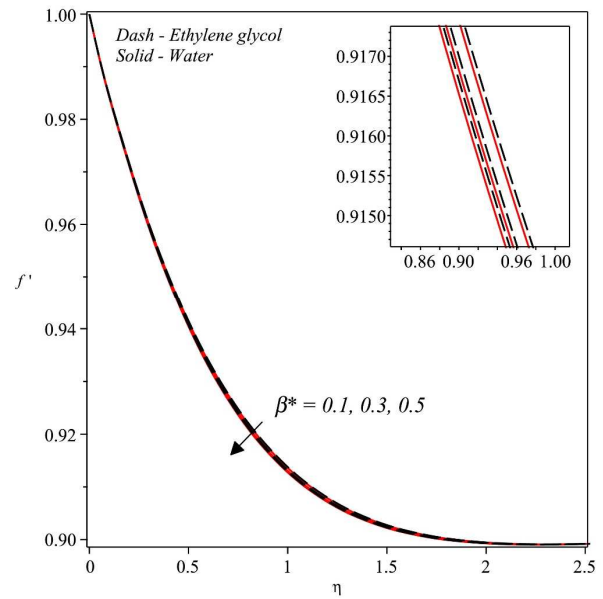
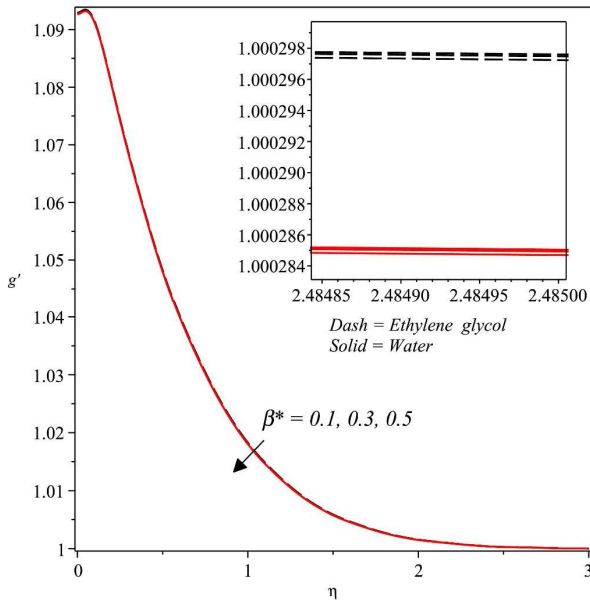
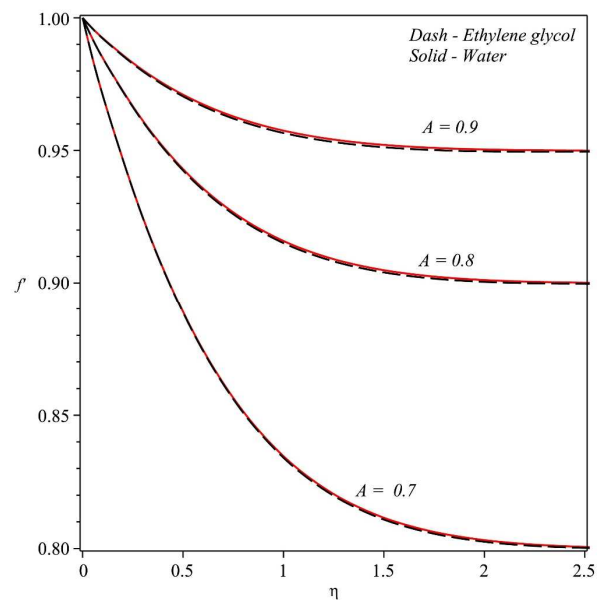
Fig. 2. Velocity curve for different  $\varepsilon$ .Fig. 3. Velocity curve for several  $\beta^*$ .Fig. 4. Induced magnetic curves for varied  $\beta^*$ .

Fig. 5. Velocity curves for numerous stretching parameter A.

Figures 5 and 6 show the nature of  $f'$  and  $g'$  for rising estimations of velocity ratio A. In Fig. 5, it has been discovered that when the parameter A level's rise, so does the flow of fluid. In fact, for larger A, the stretching rate at infinity will be larger than the stretching rate at the surface. It is observed that flow in water is escalated more than the flow in Eg. Whereas the reverse behaviour is noticed in  $g'$  in Fig. 6. Effect of  $\zeta$  on induced magnetic profile  $g'$  is portrayed in Fig. 7. It is depicted that rising  $\zeta$  corresponds to decrease in the  $g'$ . It is due to the fact that rise in the  $\zeta$  can lead hindrance in growth rate of fluid viscosity causing boundary layer thickness to deplete thereby reducing  $g'$ . From Fig. 7, the curves of  $g'$  is showing more drop in water (base fluid) than in Eg. Figures 8 and 9 demonstrate the temperature gradient profile for Ni (HSS) and thermal relaxation parameter  $\gamma_1$ . It is clear from the profile that HSS increases the temperature. Physically, the impact of the HSS augments extra energy within the boundary layer, which ultimately causes rise in the temperature. In Fig. 9, the heat profile of liquid hampers with the growth of the in  $\gamma_1$  both water and Eg. Nanoscale material particles seek a longer duration to transfer heat to their neighbouring particles as  $\gamma_1$  is increased. In Fig. 10, the influence of concentration relaxation parameter  $\gamma_2$  on concentration profile  $\chi$  for water and Eg is discussed. Due to physical properties of  $\gamma_2$ , the fluid particles will seek more time to diffuse causing declination in  $\chi$ . Figures 11 to 13 are plotted to discuss the variations in engineering coefficients  $Cf_x$ ,  $Nu_x$ , and  $Sh_x$  for porosity ( $\varepsilon$ ), HSS (Ni), and concentration relaxation parameters ( $\gamma_2$ ). As  $\varepsilon$  grows, the surface drag force falls as this produces opposition to the fluid flow due to an increase in the pore size of the medium. Hence the drop in  $Cf_x$  is observed in both water and Eg when  $\varepsilon$  is decreased in Figs. 11a and 11b. Due to physical properties of both base fluids, the drop in  $Cf_x$  is witnessed more in water than Eg. Effect of skin-friction is studied in many industrial applications such as in boundary layer transitions and heat transfer in hypersonic flow.



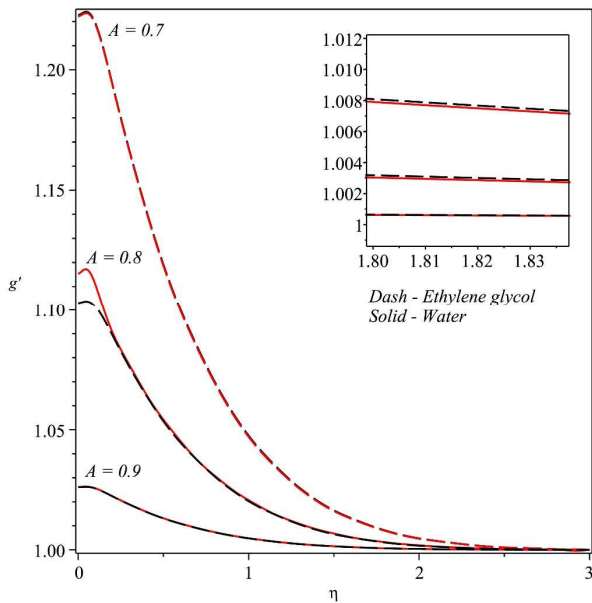


Fig. 6. Induced magnetic curves for numerous stretching parameter A.

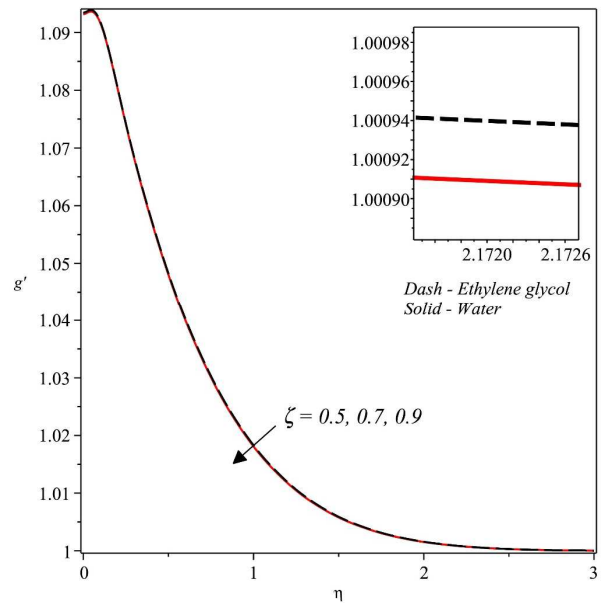
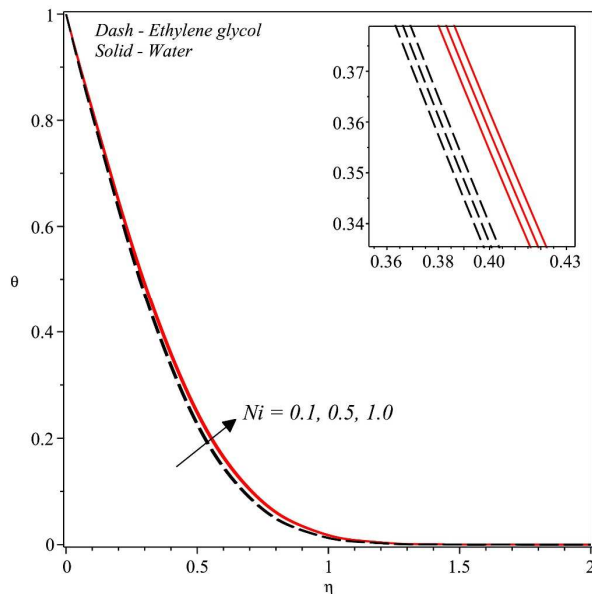
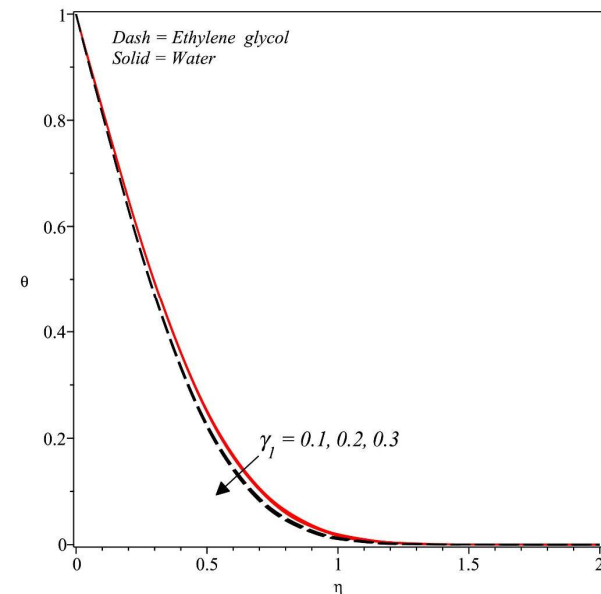
Fig. 7. Induced magnetic curves for various  $\zeta$ .

Fig. 8. Role of HSS over temperature gradient.

Fig. 9. Role of  $\gamma_1$  over temperature gradient.

Figures 12a and 12b are plotted to show the variations in  $Nu_x$  for varied values of  $Ni$  for water and  $Eg$  base fluids. On rising  $Ni$  values, increase in  $Nu_x$  is seen. Physically, the increase in the  $Ni$  generates heat energy in heat transfer process near the thermal boundary layer. Due to varied fluid characteristics of both base fluids the impact of  $Ni$  is effective in water than in  $Eg$ . Local Nusselt number is used to determine the heat transfer coefficient in fluid flow and used in missiles and spacecrafts for better thermal protection system.

Figures 13a and 13b exhibit the effect of concentration relaxation parameter ( $\gamma_2$ ) upon  $Sh_x$  for both water and  $Eg$ . A spike in the Sherwood number due to varying  $\gamma_2$  is noticed. Physically, as  $\gamma_2$  gets larger, the pace of mass transfer between a solid surface and a fluid flow accelerates. Hence an effective mass convection is seen at the surface in water compared to  $Eg$  base fluid due to its thermophysical properties. It has many industrial applications such as in distillation, extraction, drying, and absorption.

## 5. Conclusions

The effect of induced magnetic field and C-C heat flux model over a TNF flow on stretching sheet with porous medium and HSS was examined numerically. The presented graphs illustrated the impact of physical parameters on distinct profiles. All the graphs were plotted for both water and ethylene glycol base fluids. The results have been validated by the previously accessible results. Through the aforementioned findings, we acquired the following important details:

1. Velocity curves shows decreasing nature for increasing  $\varepsilon$  parameter.
2. Both velocity and induced magnetic profile displays increasing nature for varied  $\beta^*$  parameter.
3. On rising stretching parameter, it is witnessed that  $f'$  shows increasing behaviour but  $g'$  shows opposite nature.



4. Induced magnetic profile drops due to the effect of reciprocal magnetic parameter  $\zeta$ .
5. It is found that HSS promotes thermal distribution across boundary.
6. Improving relaxation time for both heat and mass flux decreases the concentration profile.

The impressive result of the current investigation could be significant and beneficial in scholarly study, particularly in clinical applications like as drug administration and electromagnetic casting.

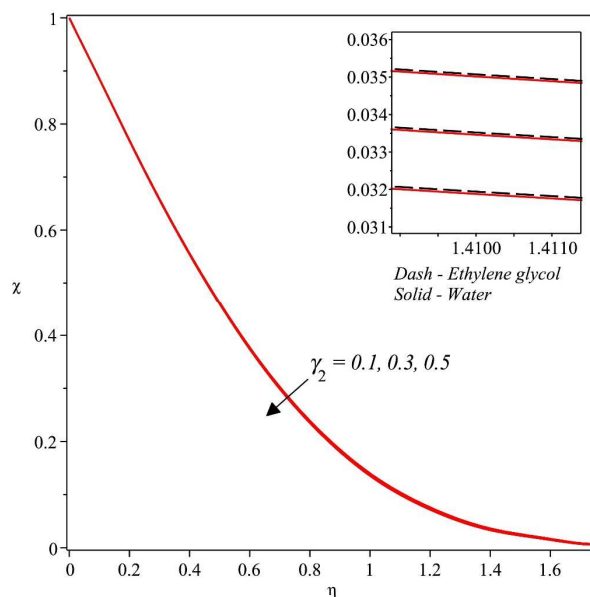
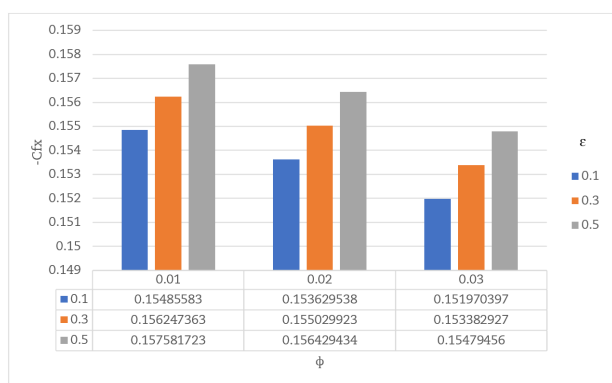
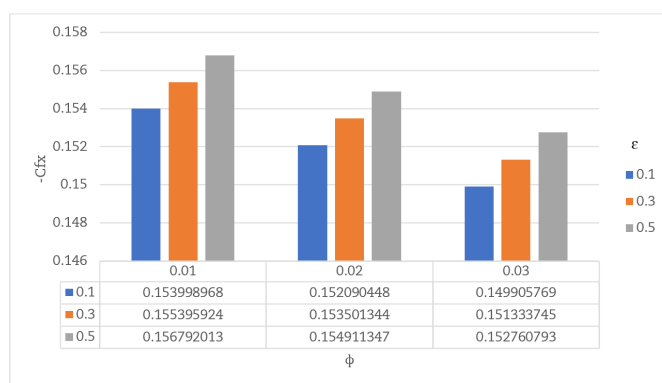


Fig. 10. Impact of  $\gamma_2$  over concentration profile.

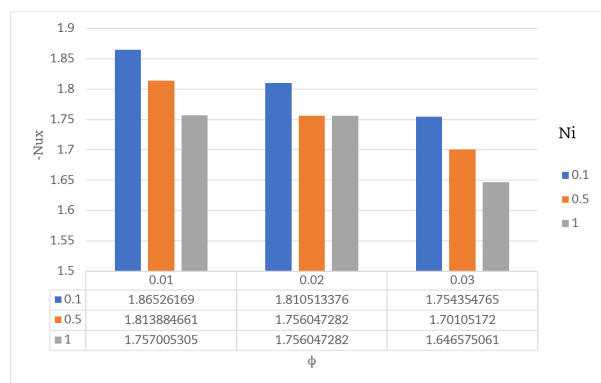


(a)

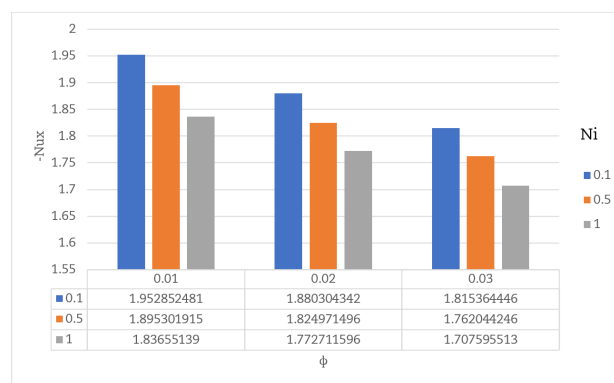


(b)

Fig. 11. Variation of  $(-Cf_x)$  for  $\epsilon$  with  $\phi$  for (a) water and (b) for Eg.



(a)



(b)

Fig. 12. Influence of Ni on  $Nu_x$  in (a) water and (b) in Eg.



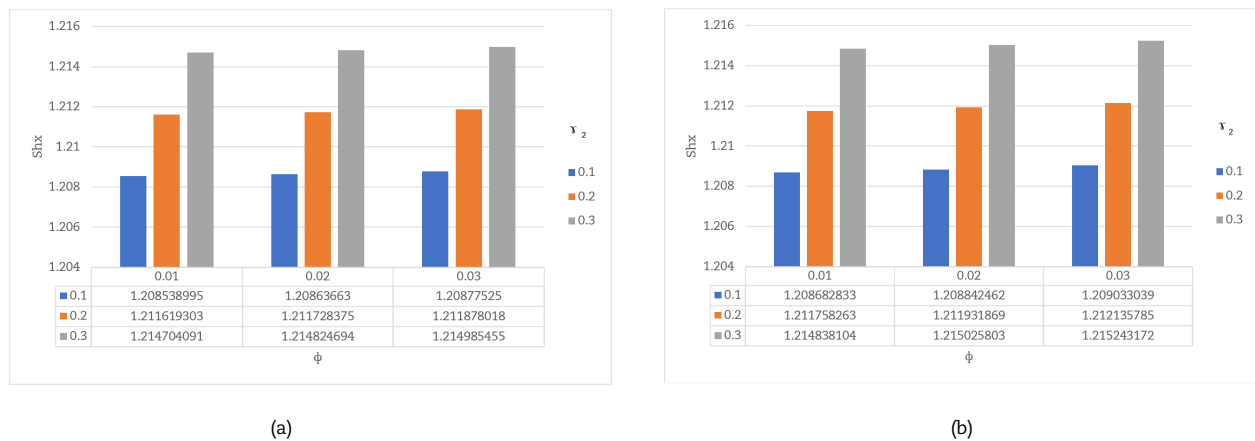


Fig. 13. Sherwood number graphs for  $\gamma_2$  in (a) water and (b) in Eg.

### Author Contributions

Formal analysis, K.M. Nihaal; investigation, U.S. Mahabaleshwar and P. Cattani; writing—original draft preparation, K.M. Nihaal; writing—review and editing, U.S. Mahabaleshwar and L.M. Pérez; All authors have read and agreed to the published version of the manuscript.

### Acknowledgements

L.M. Pérez acknowledges financial support from ANID through Convocatoria Nacional Subvención a Instalación en la Academia Convocatoria Año 2021, Grant SA77210040.

### Conflict of Interest

The authors declared no potential conflicts of interest concerning the research, authorship, and publication of this article.

### Funding

Not applicable.

### Data Availability Statements

The datasets generated and/or analysed during the current study are available from the corresponding author on reasonable request.


### References


- [1] Choi, S.U.S., Eastman, J.A., Enhancing thermal conductivity of fluids with nanoparticles, Argonne National Lab. (ANL), Argonne, IL (United States), ANL/MSD/CP-84938; CONF-951135-29, Oct. 1995, Available: <https://www.osti.gov/biblio/196525>.
- [2] Adun, H., Kavaz, D., Dagbasi, M., Review of ternary hybrid nanofluid: Synthesis, stability, thermophysical properties, heat transfer applications, and environmental effects, *Journal of Cleaner Production*, 328, 2021, 129525.
- [3] Arif, M., Kumam, P., Kumam, W., Mostafa, Z., Heat transfer analysis of radiator using different shaped nanoparticles water-based ternary hybrid nanofluid with applications: A fractional model, *Case Studies in Thermal Engineering*, 31, 2022, 101837.
- [4] Shah, N.A., Wakif, A., El-Zahar, E.R., Thumma, T., Yook, S.J., Heat transfers thermodynamic activity of a second-grade ternary nanofluid flow over a vertical plate with Atangana-Baleanu time-fractional integral, *Alexandria Engineering Journal*, 61(12), 2022, 10045–10053.
- [5] Maranna, T., Mahabaleshwar, U.S., Pérez, L.M., Manca, O., Flow of viscoelastic ternary nanofluid over a shrinking porous medium with heat Source/Sink and radiation, *Thermal Science and Engineering Progress*, 40, 2023, 101791.
- [6] Joekear-Niasar, V., Schreyer, L., Sedighi, M., Icardi, M., Huyghe, J., Coupled Processes in Charged Porous Media: From Theory to Applications, *Transport in Porous Media*, 130(1), 2019, 183–214.
- [7] Perazzo, A., Tomaiuolo, G., Preziosi, V., Guido, S., Emulsions in porous media: From single droplet behavior to applications for oil recovery, *Advances in Colloid and Interface Science*, 256, 2018, 305–325.
- [8] Mahabaleshwar, U.S., Maranna, T., Pérez, L.M., Ravichandra Nayakar, S.N., An effect of magnetohydrodynamic and radiation on axisymmetric flow of non-Newtonian fluid past a porous shrinking/stretching surface, *Journal of Magnetism and Magnetic Materials*, 571, 2023, 170538.
- [9] Mukhopadhyay, S., Heat Transfer Analysis of the Unsteady Flow of a Maxwell Fluid over a Stretching Surface in the Presence of a Heat Source/Sink, *Chinese Physics Letters*, 29(5), 2012, 054703.
- [10] Thirumalaisamy, K., et al., Comparative heat transfer analysis of  $\gamma$ -Al<sub>2</sub>O<sub>3</sub>-C<sub>2</sub>H<sub>6</sub>O<sub>2</sub> and  $\gamma$ -Al<sub>2</sub>O<sub>3</sub>-H<sub>2</sub>O electroconductive nanofluids in a saturated porous square cavity with Joule dissipation and heat source/sink effects, *Physics of Fluids*, 34(7), 2022, 072001.
- [11] Chamkha, A.J., Heat and Mass Transfer of a Non-Newtonian Fluid Flow over a Permeable Wedge in Porous Media with Variable Wall Temperature and Concentration and Heat Source or Sink, *WSEAS Transactions on Heat and Mass Transfer*, 5, 2010, 11-20.
- [12] Aslani, K.E., Mahabaleshwar, U.S., Sakanaka, P.H., Sarris, I.E., Effect of partial slip and radiation on liquid film fluid flow over an unsteady porous stretching sheet with viscous dissipation and heat source/sink, *Journal of Porous Media*, 24(11), 2021, 1-15.
- [13] Syazana Awaludin, I., Ishak, A., Pop, I., Stagnation Point Flow Over a Permeable Stretching/Shrinking Sheet with Chemical Reaction and Heat Source/Sink, *Computer Modeling in Engineering & Sciences*, 120(1), 2019, 203–214.
- [14] Acharya, N., Mabood, F., On the hydrothermal features of radiative Fe<sub>3</sub>O<sub>4</sub>-graphene hybrid nanofluid flow over a slippery bended surface with heat source/sink, *Journal of Thermal Analysis and Calorimetry*, 143(2), 2021, 1273–1289.
- [15] Sneha, K.N., Mahabaleshwar, U.S., Sharifpur, M., Ahmadi, M.H., Al-Bahrani, M., Entropy Analysis in MHD CNTS Flow Due to a Stretching Surface with Thermal Radiation and Heat Source/Sink, *Mathematics*, 10(18), 2022, 3404.




- [16] Akram, S., Athar, M., Saeed, K., Razia, A., Muhammad, T., Ahmed Alghamdi, H., Mathematical simulation of double diffusion convection on peristaltic pumping of Ellis nanofluid due to induced magnetic field in a non-uniform channel: Applications of magnetic nanoparticles in biomedical engineering, *Journal of Magnetism and Magnetic Materials*, 569, 2023, 170408.
- [17] Sheng, L., et al., Tumor Microenvironment-Responsive Magnetic Nanofluid for Enhanced Tumor MRI and Tumor multi-treatments, *Pharmaceuticals*, 16(2), 2023, 166.
- [18] Kopp, M.I., Yanovsky, V.V., Mahabaleshwar, U.S., A Bio-Thermal Convection in a Porous Medium Saturated by Nanofluid Containing Gyrotactic Microorganisms Under an External Magnetic Field, *East European Journal of Physics*, 4, 2022, 23–47.
- [19] Khan, U., Zaib, A., Ishak, A., Magnetic Field Effect on Sisko Fluid Flow Containing Gold Nanoparticles through a Porous Curved Surface in the Presence of Radiation and Partial Slip, *Mathematics*, 9(9), 2021, 921.
- [20] Sheremet, M.A., Pop, I., Rosca, N.C., Magnetic field effect on the unsteady natural convection in a wavy-walled cavity filled with a nanofluid: Buongiorno's mathematical model, *Journal of the Taiwan Institute of Chemical Engineers*, 61, 2016, 211–222.
- [21] Fourier, J.B.J., *Theorie analytique De La Chaleur*, Paris, Chez Firmin Didot, 1822.
- [22] Cattaneo, C., *Sulla conduzionedelcalore*, Atti del Seminario Maermatico e Fisico dell Universita di Modena e Reggio Emilia, 3, 1948, 83-101.
- [23] Christov, C.L., On frame indifferent formulation of the Maxwell—Cattaneo model of finite-speed heat conduction, *Mechanics Research Communications*, 36, 2009, 481–486.
- [24] Jamshed, W., Safdar, R., Ibrahim, R.W., Nisar, K.S., Eid, M.R., Alam, M.M., Shape-factor and radiative flux impacts on unsteady graphene–copper hybrid nanofluid with entropy optimization: Cattaneo–Christov heat flux theory, *Pramana*, 96(3), 2022, 163.
- [25] Israr Ur Rehman, M., et al., Effect of Cattaneo-Christov heat flux case on Darcy-Forchheimer flowing of Sutterby nanofluid with chemical reactive and thermal radiative impacts, *Case Studies in Thermal Engineering*, 42, 2023, 102737.
- [26] Hayat, T., Khan, W.A., Abbas, S.Z., Nadeem, S., Ahmad, S., Impact of induced magnetic field on second-grade nanofluid flow past a convectively heated stretching sheet, *Applied Nanoscience*, 10(8), 2020, 3001–3009.
- [27] Shah, Z., Alzahrani, E.O., Dawar, A., Alghamdi, W., Zaka Ullah, M., Entropy Generation in MHD Second-Grade Nanofluid Thin Film Flow Containing CNTs with Cattaneo-Christov Heat Flux Model Past an Unsteady Stretching Sheet, *Applied Sciences*, 10(8), 2020, 2720.
- [28] Farooq, U., Waqas, H., Khan, M.I., Khan, S.U., Chu, Y.M., Kadry, S., Thermally radioactive bioconvection flow of Carreau nanofluid with modified Cattaneo-Christov expressions and exponential space-based heat source, *Alexandria Engineering Journal*, 60(3), 2021, 3073–3086.
- [29] Wang, F., Nazir, U., Sohail, M., El-Zahar, E.R., Park, C., Thounthong, P., A Galerkin strategy for tri-hybridized mixture in ethylene glycol comprising variable diffusion and thermal conductivity using non-Fourier's theory, *Nanotechnology Reviews*, 11(1), 2022, 834–845.
- [30] Muhammad, N., Nadeem, S., Ferrite nanoparticles Ni- ZnFe<sub>2</sub>O<sub>4</sub>, Mn- ZnFe<sub>2</sub>O<sub>4</sub> and Fe<sub>2</sub>O<sub>4</sub> in the flow of ferromagnetic nanofluid, *The European Physical Journal Plus*, 132(9), 2017, 377.
- [31] Yu, Y., et al., Exploration of 3D stagnation-point flow induced by nanofluid through a horizontal plane surface saturated in a porous medium with generalized slip effects, *Ain Shams Engineering Journal*, 14(2), 2023, 101873.
- [32] Mahapatra, T.R., Gupta, A.S., Heat transfer in stagnation-point flow towards a stretching sheet, *Heat and Mass Transfer*, 38(6), 2002, 517–521.

## ORCID iD

K.M. Nihaal  <https://orcid.org/0009-0001-2432-0039>

U.S. Mahabaleshwar  <https://orcid.org/0000-0003-1380-6057>

L.M. Pérez  <https://orcid.org/0000-0002-1199-9564>



© 2024 Shahid Chamran University of Ahvaz, Ahvaz, Iran. This article is an open access article distributed under the terms and conditions of the Creative Commons Attribution-NonCommercial 4.0 International (CC BY-NC 4.0 license) (<http://creativecommons.org/licenses/by-nc/4.0/>).

**How to cite this article:** Nihaal K.M., Mahabaleshwar U.S., Pérez L.M., Cattani P. An Impact of Induced Magnetic and Cattaneo-Christov Heat Flux Model on Nanofluid Flow across a Stretching Sheet, *J. Appl. Comput. Mech.*, 10(3), 2024, 455-464. <https://doi.org/10.22055/jacm.2024.45421.4365>

**Publisher's Note** Shahid Chamran University of Ahvaz remains neutral with regard to jurisdictional claims in published maps and institutional affiliations.

